Collisional Cooling of Polar Diatomics in ^{3}He and ^{4}He Buffer Gas: A Quantum Calculation at Ultralow Energies†

E. Bodo and F. A. Gianturco*

Department of Chemistry and INFM, The University of Rome "La Sapienza", P.le A. Moro 5, 00185 Rome, Italy

Received: March 5, 2003; In Final Form: April 21, 2003

The anisotropic interactions of three polar molecules—CO, HF, and LiH—with He atoms (in their ground electronic states), obtained from accurate ab initio calculations that explicitly include their vibration-to-translation coupling terms are analyzed in detail, to compare their relative features. The quantum scattering calculations of their rotovibrational inelastic cross sections are conducted using a recently proposed multichannel treatment, the modified variable phase method, that has been implemented by the authors and applied here to ultralow collision energies. A comparison of the different relaxation efficiencies exhibited by the three title molecules in releasing their internal vibrational energy during ultracold collisions with ^{4}He and ^{3}He buffer gas is performed in detail and specific suggestions for experimental choices are extracted from these findings.

I. Introduction

There has been very rapidly growing interest recently, both experimental and theoretical, in the field of cold molecules.[1−5] Such a marked growth has been obviously inspired by the spectacular results that have been achieved in the closely related area of cold atoms, recognized in the year 2001 with the award of the Nobel Prize in physics to Cornell, Ketterle, and Wieman for achieving Bose−Einstein condensation (BEC) in dilute gases of alkali atoms. Although molecules are a much more difficult working environment for BEC experiments, it has been clear from the very beginning that they have much more to offer than simply providing an extension of the sort of experiments already performed with atoms, thereby attracting the interest of both the chemical and physical communities in trying to better understand the large variety of additional effects that are encountered on the way to bringing molecules and atom/molecule mixtures down to very low temperatures and very low velocities. Several fundamental studies[6,7] in which molecules are employed take advantage of the relative ultralow velocities between molecules that have been achieved in recent experiments. There are currently three methods that are employed to produce cold molecules that can be trapped for an acceptable length of time. One of the most widely used approaches starts with cold atoms stored in a magneto-optical trap (MOT) and, through the process of photoassociation (PA), binds two atoms together.[8−11] The ensuing molecules are translationally as cold as the atoms from which they are produced; however, because the latter bind together at rather large internuclear distances, the most favored states of the molecules formed are often high vibrational states just below their dissociation limit. Using a variety of laser schemes, the internal energy distributions of the newly formed molecules can be manipulated to transfer them to their rotovibrational and electronic ground states. In the second method, a beam of dipolar molecules is decelerated during the passage through an array of time-varying inhomogeneous electric fields[12,13] and then trapped in an electrostatic storage ring[5] or in an electrostatic quadrupole trap.[14]

Another possibility for cooling molecules is offered by injecting them in a cold helium buffer,[15−17] where they can then thermalize after a series of multiple collisions. When ^{3}He is used as a buffer gas, the temperature can be as low as 250 mK and one can still maintain a sufficient buffer gas density to ensure efficient cooling by frequent collisions. One normally expects that the target molecules would be in their electronic and vibrational ground states after the end of the equilibration process, with only a limited number of rotational states being populated. It is, therefore, of paramount importance to have some previous knowledge of the relative sizes and of the temperature behavior for the corresponding collisionally inelastic cross sections that are related to a particular molecule injected in the buffer gas to initiate the cooling step of the process. This essentially means that, to gather theoretical and, possibly, some indirect experimental information on the inelastic collisions that are occurring at ultralow temperatures, previously acquired reliable information on the anisotropic interactions that drive the collisional cooling must be available, as well as a computational tool to treat the quantum dynamics (this tool must be efficient both numerically and relative to the computer processing unit (CPU)in treating the often-numerous molecular states that can be involved in the process at hand).

In the present study, we have therefore decided to select three polar diatomics for which we have been able to obtain, from previous works,[18−20] a fairly reliable description of their full anisotropic interactions with the He atom. We shall therefore show below that the generation of numerically converged results for their collisional de-excitation cross sections at very low translational energies allows one to obtain a fairly detailed picture of the cooling efficiency for these three species in the

† Part of the special issue "Donald J. Kouri Festschrift".

* Author to whom correspondence should be addressed. E-mail: fa.gianturco@caspur.it.

10.1021/jp030303q CCC: $25.00
Published on Web 05/23/2003

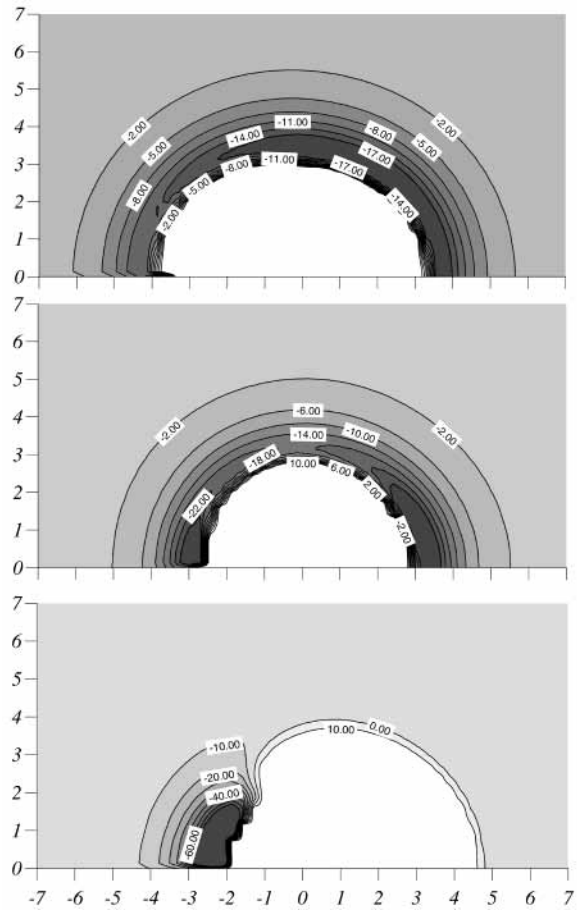

Figure 1. Energy contours for the V_{00} diagonal elements of the interaction potentials in cylindrical coordinates (the origin is located in the center of mass of the molecule) for the three systems considered here: CO (top), HF (middle), and LiH (bottom). Distances are given in angstroms and energy levels are given in units of cm^{-1}.

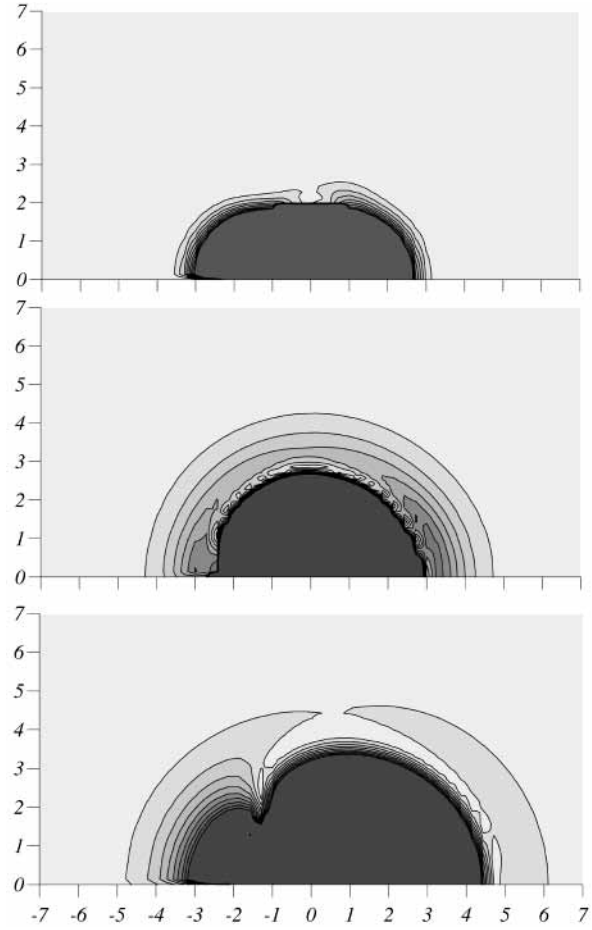

Figure 2. Energy contours of the $|V_{01}|$ off-diagonal elements of the interaction potentials in cylindrical coordinates (the origin is located in the center of mass of the molecule) for the three systems considered here: CO (top), HF (middle), and LiH (bottom). Distances are given in angstroms. The minimum contour level is located at 0 cm^{-1}, and each of the contours is plotted every 5 cm^{-1}. Darker areas correspond to stronger couplings.

chosen buffer gas and also makes it possible to suggest the environmental parameters that would help to optimize the working conditions in experiments. In the next section, we present and discuss the relative features of the three potential energy surfaces (PESs), whereas in Section III, we give theoretical and computational details of the method that we have implemented to solve the quantum coupled equations of the inelastic dynamics. The present results are displayed and discussed in Section IV, and our final conclusions and future plans are reported in Section V.

II. Potential Energy Surfaces

To attempt a comparison of the dynamical behavior of the three title systems, a short analysis of their PESs is required. Two of the three PESs—CO + He[18] and HF + He[19]—have been calculated using the symmetry-adapted perturbation theory (SAPT) method, whereas the LiH + He surface was obtained instead using the MP2 method with a CCSD(T) correction.[20] In Figure 1, we report the energy contours of the lowest adiabatic coupling element obtained from the PESs, namely, the numerical results from taking the integral $\int_0^\infty \chi_0(r)V(r,R,\theta)\chi_0(r)\,dr$ that returns a $V_{00}(R,\theta)$ PES. For nonreactive systems, such quantities are very similar to the simpler rigid rotor interaction $V(r_{eq},R,\theta)$. In each of the panels, the PES for $R < 2.0$ Å is not shown.

Figure 1 clearly shows that the three systems have completely different interaction profiles: the CO surface (top panel) is almost isotropic and has a well depth of approximately -20 cm^{-1}; the HF interaction is much less isotropic, showing the presence of two similar wells of approximately -35 cm^{-1} at 0° and 90°; the LiH−He surface (bottom panel), on the other hand, is very anisotropic. This is partly due to the large mass difference between lithium and hydrogen that places the LiH center-of-mass very close to the Li atom, and partly because the LiH electronic structure resembles a Li^+H^- ion-pair state with a very anisotropic electron density distribution. The potential well is also much deeper here and reaches -180 cm^{-1} on the Li side of the target.

We are interested in analyzing the vibrational relaxation cross sections at ultralow energies; therefore, in Figure 2, we report the corresponding contour levels for the modulus of the first off-diagonal element $|V_{01}|$. In all the panels, the coupling is not shown for values of $R < 2.0$ Å. This scenario gives a qualitative idea of the strength of the vibrational coupling that acts during the collision: in CO, the vibrational coupling is small and appreciable only at very short range; on the other hand, it is stronger in HF and extends to larger distances; in the LiH−He system, the vibrational-to-translational coupling is rather strong, acts over a wide range of distances, and is markedly localized on the lithium side.

The features of the PESs that we briefly analyzed previously are confirmed by the well-known dynamical behavior of these

systems, gathered from the large amount of calculations on the rotovibrational excitation of the target (see Antonova et al.[21] for data regarding the CO−He PES and Bodo et al.[22] for data regarding the LiH−He PES) at room temperature and on its relaxation cross sections.[23,24]

III. Quantum Dynamics

The time-independent formulation of any close coupling (CC) approach to quantum inelastic scattering is certainly well-known and will be not repeated here. Two problems, however, arise when ultralow collision energies are involved: (i) the large range of integration of the CC equations that is required and (ii) the number of steps requested by the integrator, which becomes very large. An integrator that can adapt its step size at long range (when the potential usually becomes monotonic and smooth) is a good choice for this type of problem, although it would be much better if the same integrator were also able to reduce the number of channels during the outward propagation. We have recently published an algorithm for the solution of the CC equation[25] that modifies the variable phase approach[26] to solve that problem, specifically addressing the latter point.

A. Variable Phase Algorithm. The time-independent scattering eigenstates of a system, here denoted as $\Psi^{i,+}$, are usually expanded in terms of diabatic target eigenstates:

$$\Psi^{i,+}(R,x) = \sum_f F_{i\rightarrow f}(R) X_f(x) \tag{1}$$

where i denotes the (collective) initial states of the colliding partners and the X_f terms are the eigenstates of the isolated molecules (channel eigenstates). The $F_{i\rightarrow f}$ terms are the channel components of the scattering wave function, which must be determined by solving the Schroedinger equation, subject to the usual boundary conditions:

$$F_{i\rightarrow f}(R) \rightarrow \delta_{if} h^{(-)}(R) - S_{fi} h^{(+)}(R) \quad \text{as} \quad (R\rightarrow\infty) \tag{2}$$

where f denotes a channel that is asymptotically accessible at the selected energy (open channel) and $h^{(\pm)}$ is a pair of linearly independent free-particle solutions. Usually, one considers a single angular momentum J at the time: when $h^{(\pm)}$ are chosen to be the appropriate Riccati−Hankel functions, the coefficients S_{fi} are the elements of the partial wave reduced-scattering matrix, often denoted as $\boldsymbol{S}^J$. In principle, the sum in eq 1 should span the relevant discrete spectrum of the isolated molecules and, whenever possible, also its continuum portion. Usually, however, numerically converged scattering observables are obtained by retaining only a limited number of discrete channels. The number of channels to be included in the expansion of the wave function is dependent strongly on the system and the collision energy. However, for a given collision energy, it is also dependent on the value of the radial scattering coordinate: at short range, where the interaction is strong, the set of channels should include at least all the channels that are energetically accessible when one considers the attractive features of the potential (a number that can be very large and usually includes several closed channels). In the asymptotic region, where the interaction is absent, only open channels are needed. Between these two extreme situations is a region that can be quite large, in the case of long-range potentials, in which the closed channels at higher energies are increasingly less important and, as will be shown in the following, can be neglected without any loss of accuracy. The usual coupled equations in the space-fixed (SF) reference frame of the multichannel scattering problem for M channels can be expressed as

$$\left\{\frac{\mathrm{d}^2}{\mathrm{d}R^2} + \boldsymbol{k}^2 - \boldsymbol{V} - \frac{\boldsymbol{l}^2}{R^2}\right\}\boldsymbol{g} = 0 \tag{3}$$

where $[\boldsymbol{k}^2]_{ij} = \delta_{ij} 2\mu(E - \epsilon_i)$ is the diagonal matrix of the asymptotic (squared) wavevectors, $[\boldsymbol{l}^2]_{ij} = \delta_{ij} l_i(l_i + 1)$ the matrix representation of the square of the orbital angular momentum operator, $\boldsymbol{g}$ a column vector that holds the radial F's channel components of the scattering wave function. The parameter $\boldsymbol{V}$, defined as $\boldsymbol{V} = 2\mu\boldsymbol{U}$, represents the potential coupling matrix whose elements, in the case of atom-vibrating diatom scattering, are given as

$$2\mu \sum_\lambda V_\lambda(\nu',\nu';R) f_\lambda(j,l,j',l',J) \tag{4}$$

where the f_λ terms are the Percival and Seaton coefficients[27] and

$$V_\lambda(\nu,\nu';R) = \int_0^\infty \mathrm{d}r \chi_{\nu'}(r) V_\lambda(R,r) \chi_\nu(r) \tag{5}$$

where the interaction potential has been expanded in Legendre polynomials $V(R,r,\theta) = \sum_\lambda V_\lambda(R,r) P_\lambda(\cos\theta)$. The two coupling terms with $(\nu,\nu') = (0,0)$ and $(\nu,\nu') = (0,1)$ are those reported in Figures 1 and 2.

The M, linearly independent solution vectors obtained with the regular condition $\boldsymbol{g}(0) = 0$ form a matrix solution Ψ; one usually defines the additional log-derivative matrix $\boldsymbol{Y} = \Psi'\Psi^{-1}$ (where variables with a prime symbol denote a derivative, with respect to R), which is invariant for (nonsingular) linear combinations of the solution vectors and satisfy the well-known Riccati matrix equation

$$\frac{\mathrm{d}\boldsymbol{Y}}{\mathrm{d}R} + \boldsymbol{W} + \boldsymbol{Y}^2 = 0 \tag{6}$$

in which $\boldsymbol{W} = \boldsymbol{k}^2 - \boldsymbol{V} - \boldsymbol{l}^2/R^2$. One solves eq 6 for $\boldsymbol{Y}$, beginning with the condition $\boldsymbol{Y}^{-1} = 0$, in place of solving eq 3 for the solution matrix Ψ, because, in this way, one avoids the need to stabilize the wave function against linear dependence of the solution vectors. The scattering observables are obtained in the asymptotic region where the log-derivative matrix has a known form, in terms of free-particle solutions and unknown mixing coefficients. For example, in the asymptotic region, the solution matrix can be written in the form

$$\Psi(R) = \boldsymbol{J}(R) - \boldsymbol{N}(R)\boldsymbol{K} \tag{7}$$

where $\boldsymbol{J}(R)$ and $\boldsymbol{N}(R)$ are matrixes of the Riccati−Bessel and Riccati−Neumann functions.[28]

The $\boldsymbol{K}$ matrix defines a set of mixing coefficients of the free-particle solutions. It is an "augmented" reactance matrix, whose open−open block holds all the scattering information and is related to the scattering matrix $\boldsymbol{S}$ by a Caley transformation (see, for example, Taylor[29]). Therefore, at the end of the propagation, one uses the log-derivative matrix to obtain the $\boldsymbol{K}$ matrix by solving the following linear system:

$$(\boldsymbol{N}' - \boldsymbol{Y}\boldsymbol{N})\boldsymbol{K} = \boldsymbol{J}' - \boldsymbol{Y}\boldsymbol{J} \tag{8}$$

The $\boldsymbol{Y}$-to-$\boldsymbol{K}$ transformation given by eq 8 can be used at each *R to define* a $\boldsymbol{K}(R)$ matrix: this matrix is the augmented $\boldsymbol{K}$ matrix for the potential truncated at R. A differential equation

for $\boldsymbol{K}(R)$ can then be written:

$$\boldsymbol{K}' = -\Psi^{\dagger}\boldsymbol{V}\Psi \tag{9}$$

where $\Psi = \boldsymbol{J} - \boldsymbol{N}\boldsymbol{K}$. (See Appendix A of ref 25.) This is the $\boldsymbol{K}$-matrix variable phase equation, and it is equivalent to eq 6.

Unlike that in the log-derivative formalism, all the $\boldsymbol{K}$-matrix elements are not equally important. Clearly, we are mainly interested in the open−open block of the matrix; in particular, in the asymptotic region, we are *only* interested in that block. The other blocks of the matrix must be considered only to the extent to which they influence the open−open block. Having a clear separation between the physical and virtual spaces, one may argue that, when the virtual contributions to the physical space become negligible, the virtual space can then be reduced. This is the basis of our channel reduction procedure, which we have described in detail in ref 25.

To solve the ordinary differential equation (ODE) problem, we choose a fifth-order embedded Runge−Kutta method. In this way, one obtains a fourth-order solution and an estimate of the truncation error. If the error is less than a preselected threshold value, Δ_{ij} (for each (i, j) element), its value is used to *increase* the step size for the next step. Therefore, we adopt, in this way, a variable step-size integration. The channel reduction procedure is used on the energy shell each time, i.e., on the closed channels with the same highest wavevector k_i. The contribution of this shell to the open−open block is checked during the propagation, and when its contribution is small, all the channels of the shell are eliminated (for details, see ref 25).

B. Ultralow Energy Scattering. The de-excitation collisions that will be analyzed here are inelastic collisions that occur in the ultralow kinetic energy regime. In the entrance channel, the molecule is in a vibrational excited state ($\nu = 1$ or $\nu = 2$) and in its ground rotational state, and the open channels in the limit of zero initial kinetic energy are all the rotovibrational levels with $E < E(\nu, j = 0)$. Because the collision is inelastic (the molecule undergoes a relaxation to a lower energy level), the elastic phase shift is a complex number and we can define a complex scattering length as the limiting value of $\delta_\nu(k)/k$ when $k \rightarrow 0$, where k is the initial wavevector associated to the initial kinetic energy. Expanding the elastic element $S_{\nu\nu'}$ in powers of k, we have

$$S_{\nu\nu'} \simeq 1 + 2i\delta_\nu(k) = 1 - 2ik(\alpha_\nu - i\beta_\nu) = 1 - 2ika_\nu \tag{10}$$

so that the knowledge of the elastic element of the $\boldsymbol{S}$ matrix when $k \rightarrow 0$ allows us to calculate the real (α_ν) and imaginary (β_ν) portions of the scattering length a_ν.[30,31] Total inelastic and elastic cross sections in the $k \rightarrow 0$ limit can then be easily calculated and are given by

$$\sigma_\nu^{\mathrm{el}} = 4\pi|a_\nu|^2$$

$$\sigma_\nu^{\mathrm{in}} = \frac{4\pi\beta_\nu}{k} \tag{11}$$

where the second expression is just the well-known Wigner's threshold law for inelastic collisions. Integration of the second expression with a Maxwellian distribution of the velocities gives the limiting constant value for the total quenching rate coefficient:

$$R_\nu(T \rightarrow 0) = \frac{4\pi\hbar\beta_\nu}{\mu} \tag{12}$$

The scattering length can also be used to estimate the position and width of any resonance that exists in the entrance channel. The analytically continued $\boldsymbol{S}$ matrix has a pole at a point k_p located in the complex k-plane. Both the imaginary and real portions of k_p can be calculated in terms of the scattering length contributions and are given by

$$\mathscr{T}(k_\mathrm{p}) = \frac{\alpha_\nu}{|a_\nu|}$$

$$\mathscr{R}(k_\mathrm{p}) = -\frac{\beta_\nu}{|a_\nu|} \tag{13}$$

We can thus obtain the complex energy value E_p of the resulting $\boldsymbol{S}$-matrix pole, on one of the two Riemann sheets of the twofold complex energy plane, using the formula

$$E_\mathrm{p} = \frac{k_\mathrm{p}^2}{2\mu} = -\frac{\exp[-i2\arctan(\beta_\nu/\alpha_\nu)]}{2\mu|a_\nu|^2} = E - \left(\frac{i}{2}\right)\Gamma \tag{14}$$

The real portion of eq 14 gives the energy of the bound ($\alpha > 0$) or virtual ($\alpha < 0$) state. We are dealing with an inelastic collision, because the initially excited molecule may undergo rotovibrational quenching; therefore, the energy of the bound or virtual states has an associated width that is given by $\mathscr{T}(E_\mathrm{p}) = \Gamma$, so that the state becomes metastable and its lifetime is $\tau = 1/\Gamma$.[30]

IV. Vibrational Relaxation Dynamics

The calculations have been performed over a wide range of collision energies (from 10^{-7} to 1 cm^{-1}) that includes the Wigner's law regime and energies at which the first shape resonances appear, which is a region that represents a situation in which the behavior of the cross sections changes completely from the ultracold regime. The state-to-state rotovibrational cross sections from $\nu = 2$ and $\nu = 1$ have been calculated using a full CC approach and both ^{3}He and ^{4}He; however, here, we will limit the discussion only to rotationally summed cross sections, because the detailed analysis of the large amount of data is still in progress and will be reported elsewhere. For each of the systems, a constant step-size log-derivative[32] propagation has been used, up to 10 Å, where the first R-dependent $\boldsymbol{K}$ matrix has been calculated. From that point, the outward propagation was conducted, using the variable phase equations, up to $R =$ 100 Å, for each system. The number of total steps employed is variable and dependent both on the nature of the system and on the collision energy; however, for the lowest energies, it was on the order of 4000. For each system, only s-wave (total angular momentum of $J = 0$) calculation was performed, up to a collision energy of 10^{-3} cm^{-1}; for larger energies, all the necessary values of the total angular momentum were calculated (6 for CO, 4 for HF and LiH). The number of states employed in the CC expansion was dependent on the nature of the system and on the strength of its rotovibrational coupling: for CO, the first three vibrational states were included and $j_{\max}$, the maximum rotational molecular state, was chosen to be 25; for HF and LiH, five vibrational states were used with $j_{\max} = 20$ and 25, respectively. This resulted in a total of 78, 105, and 130 asymptotic coupled channels in each calculation. When considering the vibrational relaxation from $\nu = 1$, the highest closed rotational channels were not employed, thus reducing the number of channels to 53, 65, and 80, whereas the same number of coupled vibrational states was retained. Most of the

TABLE 1: Computed Quantities from the *s*-wave Cross Sections and *S* Matrix[a]

system	α_ν (a.u.)	β_ν (a.u.)	E (cm^{-1})	τ (s)	R_ν ($cm^3 \cdot s^{-1}$)
$CO(\nu = 2) + {}^3He$	3.9	7.3×10^{-9}	−0.40	4.2×10^{-4}	2.13×10^{-19}
$CO(\nu = 2) + {}^4He$	**−5.4**	5.7×10^{-10}	**−0.17**	1.8×10^{-2}	1.29×10^{-20}
$CO(\nu = 1) + {}^3He$	4.5	4.6×10^{-9}	−0.31	4.1×10^{-3}	1.3×10^{-19}
$CO(\nu = 1) + {}^4He$	**−4.4**	2.3×10^{-10}	**−0.24**	1.0×10^{-1}	5.3×10^{-21}
$HF(\nu = 2) + {}^3He$	1.8	8.5×10^{-5}	−2.0	3.3×10^{-9}	2.6×10^{-15}
$HF(\nu = 2) + {}^4He$	**−2.8**	2.7×10^{-4}	**−0.62**	-5.4×10^{-9}	6.5×10^{-15}
$HF(\nu = 1) + {}^3He$	1.7	1.0×10^{-5}	−2.3	9.3×10^{-8}	3.1×10^{-16}
$HF(\nu = 1) + {}^4He$	**−3.1**	3.4×10^{-5}	**−0.51**	-2.4×10^{-7}	8.1×10^{-16}
$LiH(\nu = 2) + {}^3He$	6.1	9.8×10^{-2}	−0.20	9.9×10^{-11}	3.6×10^{-12}
$LiH(\nu = 2) + {}^4He$	2.4	4.9×10^{-1}	−0.95	1.6×10^{-12}	1.5×10^{-11}
$LiH(\nu = 1) + {}^3He$	5.8	2.4×10^{-3}	−0.22	1.4×10^{-8}	9.0×10^{-14}
$LiH(\nu = 1) + {}^4He$	1.3	1.2×10^{-2}	−3.44	4.0×10^{-11}	3.8×10^{-13}

[a] See text for the meanings of the symbols.

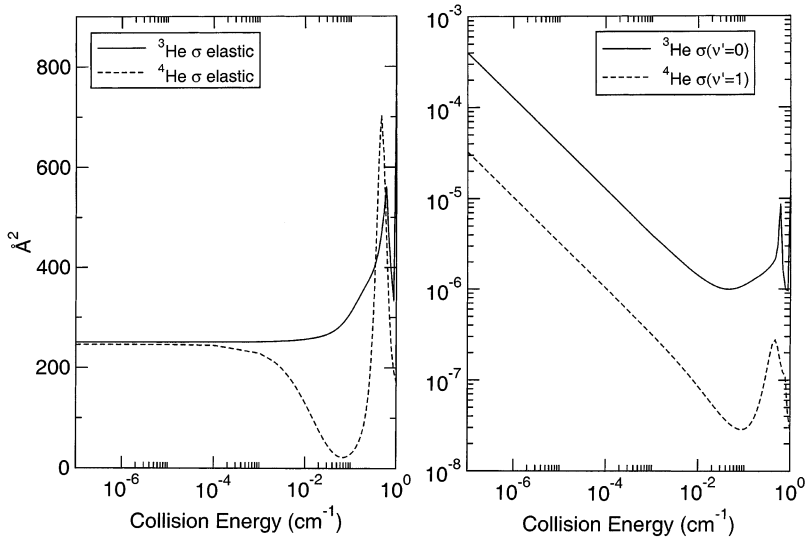

Figure 3. Vibrational quenching (right panel) and elastic (left panel) cross section for $CO(\nu = 1) + {}^3He$ and $CO(\nu = 1) + {}^4He$.

closed channels were eliminated during the outward propagation, because they have some importance only in the stronger interaction region. For example, for $HF(\nu = 2, j = 0) + {}^3He$ at 10^{-7} cm^{-1}, the number of channels was reduced from 105 at $R = 10$ Å to 39 at $R = 24$ Å, while retaining an accuracy of 10^{-5} on the elements of the open−open block of the $\boldsymbol{K}$ matrix.

The *s*-wave elastic and inelastic cross sections, determined at 10^{-7} cm^{-1}, have been used to calculate the real and imaginary portions of the scattering length using eqs 11. The *s*-wave $\boldsymbol{S}$ matrix was then used to determine the sign of α. These and the other quantities described in the previous section are reported in Table 1. Some of the scattering lengths are determined to be negative (bold numbers in the table), which means that some of the interaction potentials are not able to accommodate a true metastable state near the threshold. Thus, the resulting computed energies E are those of a virtual state living on the nonphysical Riemann sheet of the complex energy plane. At the same time, the lifetimes of the collision complexes are marked as negative as it happens in electron−molecule scattering when a Ramsauer−Townsend effect takes place.[33]

The results that we find here for the CO + He system are similar to those reported by Zhu et al.[34] and Balakrishnan et al.,[35] both for the scattering lengths and for the total quenching rates. The differences probably result from the fact that, here, we have used simpler *j*-independent vibrational wavefunctions to generate the potential coupling elements.

All the quantities reported in Table 1 confirm that the LiH molecule is, by far, the one with the largest rate coefficient for the vibrational de-excitation and the one with the shortest lifetimes. This result indicates that LiH is an ideal candidate molecule to be vibrationally and rotationally cooled by collision with a helium buffer gas.

A. Vibrational Relaxation Cross Sections for $\nu = 1$. First, we report the de-excitation results from $\nu = 1$. In Figures 3−5, the elastic and the vibrational quenching cross sections[36] are plotted as a function of the collison energy.

The Wigner's regime is established at different energies, depending on the nature of the system. The one for which it settles at the highest energies is LiH + ^{3}He, as can be seen from the left panel of Figure 5. However, for each of the systems considered here, at a collision energy of 10^{-4} cm^{-1}, all the collision properties can be safely assumed to be determined only by the knowledge of the complex scattering length (i.e., following eqs 11). For CO and LiH, shape resonances are clearly visible at the higher energies sampled by our calculations, and, in both cases, wave analysis reveals that it is the $J = 2$ total angular momentum that gives rise to the shape resonance and, because the initial angular momentum of the molecule is zero, the resonance is due to a partial wave component with an orbital angular momentum of $l = 2$. A plot of the various partial wave contributions to the total cross section for the latter system is reported in Figure 6. From the same figure, it is clear to see when the regime of "quantum suppression" of the $l \neq 0$ contributions to the total cross section is established: it already occurs at energies of 10^{-2} cm^{-1}.

The $CO(\nu = 1)-{}^4He$ and $CO(\nu = 1)-{}^3He$ systems have already been analyzed in two earlier papers,[34,35] where it was also found that the quenching cross section for He−CO is rather

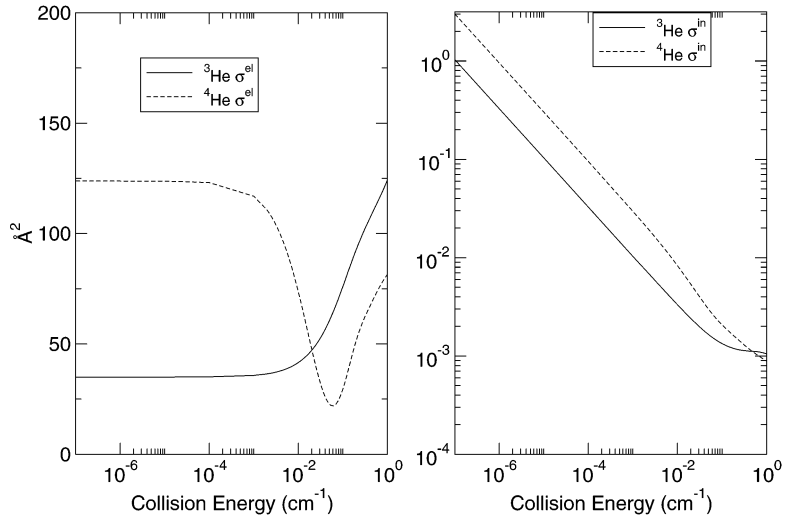

Figure 4. Vibrational quenching (right panel) and elastic (left panel) cross section for HF($\nu = 1$) + ^{3}He and HF($\nu = 1$) + ^{4}He.

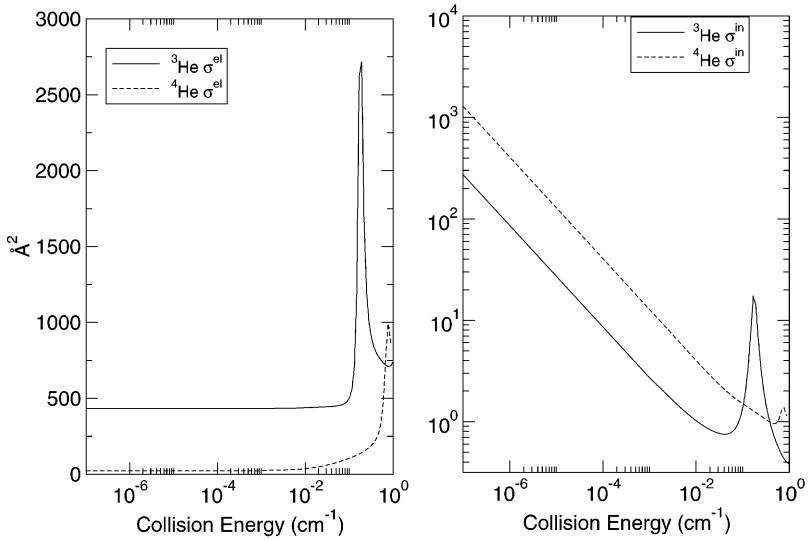

Figure 5. Vibrational quenching (right panel) and elastic (left panel) cross section for LiH($\nu = 1$) + ^{3}He and LiH($\nu = 1$) + ^{4}He.

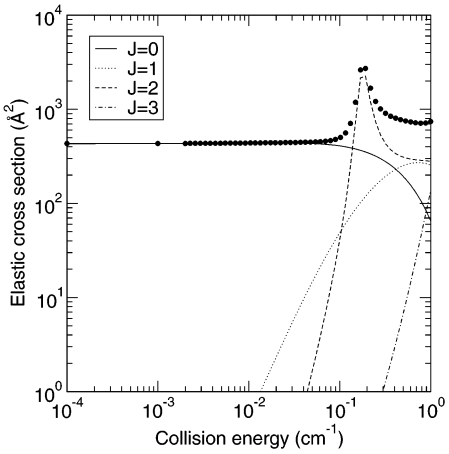

Figure 6. Partial wave contributions to the total cross section (filled circles) for LiH($\nu = 1$) + ^{3}He.

small. This is a reasonable result, given the large mass of the CO molecule and the small degree of vibrational coupling, which we have already discussed in Section II. The limiting values of the rate constants reported in Table 1 and the cross sections that we find here for CO−He are similar to those reported in refs 34 and 35.

If we now turn our attention to the HF molecule, we see that the elastic cross sections obtained with the bosonic helium are much larger than those with ^{3}He, which is a behavior that might be due to the presence of a virtual state near the threshold, as indicated by the large and negative value of the scattering length in Table 1. The corresponding Ramsauer minima can be seen for energies in the range of $10^{-2}-10^{-1}$ cm^{-1}. The two quenching cross sections differ by the same factor as the elastic ones, so that the one with ^{4}He is only a factor of 3 larger than that with ^{3}He. Moreover, the HF system seems to be free from shape resonances at the energies considered here.

The LiH case is still different from the other two: here, the ^{3}He elastic cross section is very large, with respect to the particularly low cross section that comes from the calculation with ^{4}He. The probable reason for this behavior is related to the presence of a bound state very near the threshold that should be much more spatially diffuse in the ^{3}He case (given the appreciable difference in the values of their scattering lengths shown in Table 1). It is also interesting to note that the LiH + He collisions exhibit the largest inelastic cross sections here. In the last column of Table 1, the limiting value of the quenching

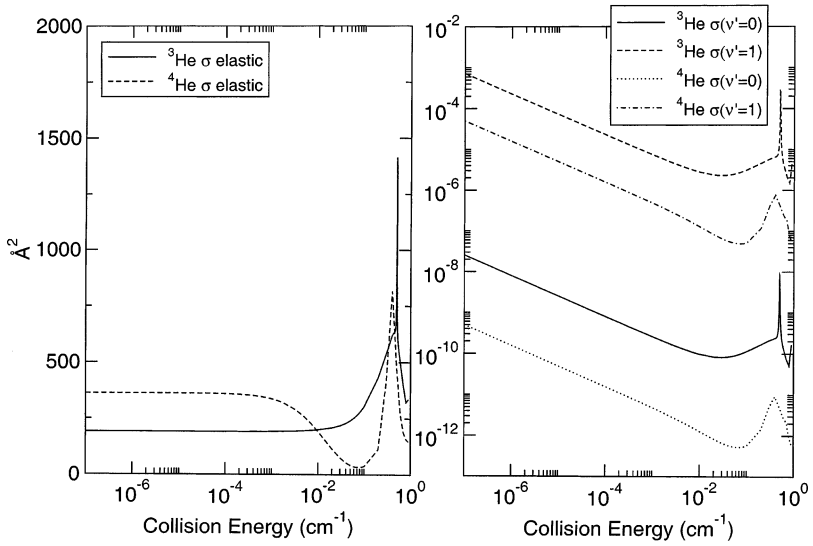

Figure 7. Vibrational quenching (right panel) and elastic (left panel) cross section for CO($\nu = 2$) + ^{3}He and CO($\nu = 2$) + ^{4}He.

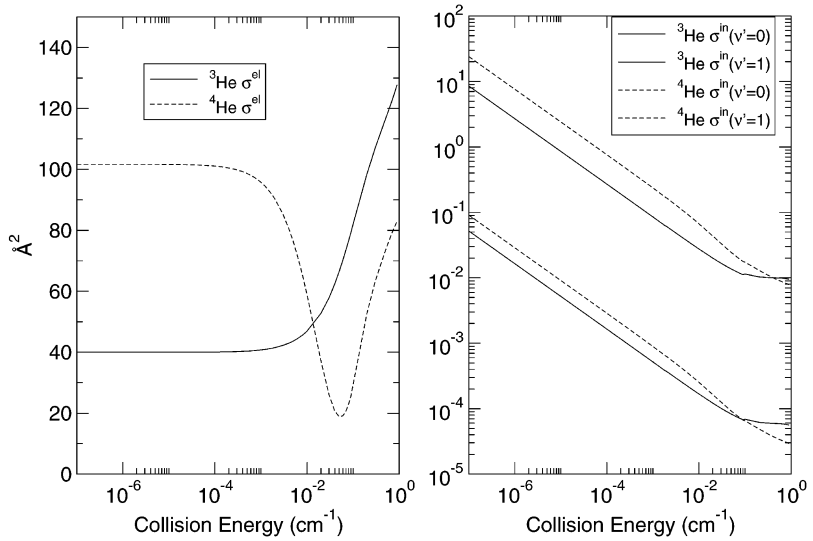

Figure 8. Vibrational quenching (right panel) and elastic (left panel) cross section for HF($\nu = 2$) + ^{3}He and HF($\nu = 2$) + ^{4}He.

rate constants are reported: one can see how the LiH + He system shows the largest quenching rate constant, at least when using the PES employed here. From this viewpoint, therefore, LiH seems to be the best candidate for undergoing efficient sympathetic cooling with helium as a buffer gas.

B. Vibrational Relaxation Cross Sections for $\nu = 2$. In Figures 7−9, we show the computed elastic and inelastic cross sections that are due to the vibrational quenching collisions from the second excited vibrational state ($\nu = 2$) of the three molecules.

There are now two possible quenching processes during which the molecule can release its vibrational energy content: a two-quanta vibrational jump and a single quantum jump. In all three systems, the $\Delta\nu = 2$ jump is less efficient than the single quantum exchange, as should be expected for van der Waals systems and from simple energy-gap consideration (for example, see Gianturco[37]); however, although the difference is only 2 orders of magnitude for HF, it increases to 4 orders of magnitude for LiH and even larger for CO. We note that the results reported here for CO−He differ from those reported by Bodo et al.[38] by a factor of 20 at low energies. The disagreement between the two sets of results is due to an overestimation of the long-range portion of the potential done in ref 37. This expected behavior can be explained in simple terms when considering the relative strength of the V_{01} and V_{02} vibrational coupling elements for all three systems (for a detailed discussion of this type of effect in H + H_2, see ref 31). When one compares these findings to those for the collisional de-excitation from the $\nu = 1$ level previously discussed, one finds that the quenching cross sections and the corresponding rate constants are, in general, larger in the present $\nu = 2$ case, because now the molecule have two routes to release the internal energy (strictly speaking, many more relaxation routes exist, because there are several rotational channels below the initial state that are energetically available) and also because the vibrational relaxation from higher levels is more efficient,[31,39] as expected from the reduction of the energy gap when going to excited states (for example, see ref 37).

Although now the molecule has a greater internal energy content, the elastic cross-section profiles (and, therefore, the real portion of the scattering length) for the calculations that start with $\nu = 2$, and those that start with $\nu = 1$ reported in the previous section, are very similar, both in shape and absolute magnitude. In each case, the $\nu = 1$ and $\nu = 2$ elastic processes indeed show the appearance of very similar shape resonances in the higher-energies regime. As we have mentioned previously, some of the scattering lengths reported in Table 1 have negative values (they are shown in boldface type), and, therefore, the

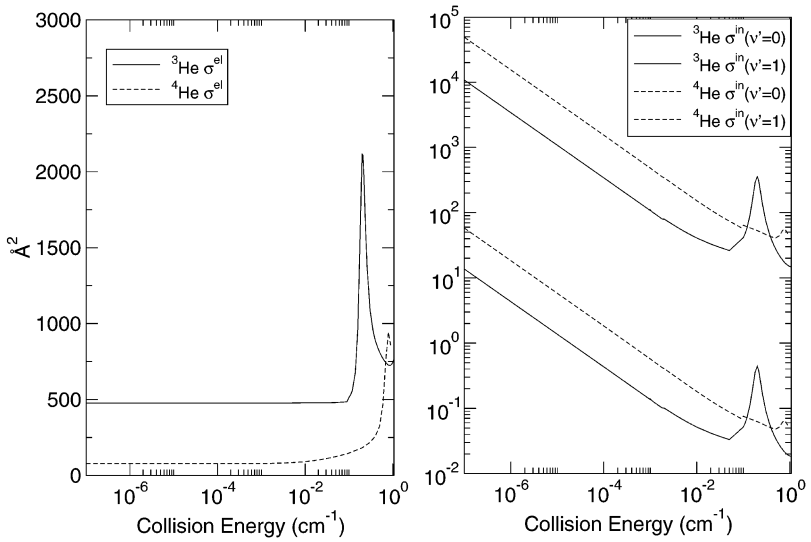

Figure 9. Vibrational quenching (right panel) and elastic (left panel) cross section for LiH($\nu = 2$) + ^{3}He and LiH($\nu = 2$) + ^{4}He.

collisional systems for which this happens also exhibit, in the elastic cross sections, marked Ramsauer minima that are due to the vanishing of the *s*-wave contribution to the total cross section at energies where that partial wave is still the largest that contributes to that cross section. Another external or experimental quality check of the PESs, which we have employed here, might come first from a possible detection and measurement of such minima. This point is rather interesting, because another feature that makes LiH a good candidate for collisional cooling (at least as it is described by the interaction employed here) is also the absence of such minima in our calculations. They, in fact, might make the helium buffer gas completely "transparent" to molecules at some particular kinetic energy, thereby reducing the efficiency at which these molecules thermalize with the chosen buffer gas.

V. Present Conclusions

In this work, we have discussed, in some detail, the computational behavior of the vibrational relaxation cross sections, summed over all their final rotational transitions, for specific diatomic molecules such as CO, HF, and LiH (with increasing permanent dipole moment) at ultralow collision energies. These molecules have been considered to relax collisionally in a buffer gas of either ^{3}He or ^{4}He atoms, and the corresponding calculations have been performed using a rigorous close-coupling approach within a quantum treatment of the dynamics. The aim of this work was to establish, via a reliable treatment of the relaxation dynamics, the possible differences that exist among these three molecules, in terms of the relative efficiency of collisional cooling within a cold buffer gas as the one often experimentally proposed and used for this purpose.[15−17] Hence, we have endeavored to first describe the interaction forces between the title systems and the He atom (all being dominated by fairly weak van der Waals interactions), using potential energy surfaces (PESs) (that are as accurate as possible) for which the vibrational coupling terms were also available.[18−20] An analysis of the main features of the interaction forces, at the level of accuracy accessible with the present calculations, revealed the following:

(1) The variations of polarity when going from C−O to Li−H reflect themselves rather clearly on the angular dependence (orientational anisotropy) variations exhibited by the three systems: only a weak dependence on θ is observed in the case of CO−He, whereas the dependence becomes markedly stronger for LiH−He.

(2) The corresponding vibration-to-translation coupling potentials reflected by the behavior of the $V_{\nu\nu}(\theta, R)$ PESs discussed in Section II also vary rather markedly when going from CO−He to LiH−He; in the latter case, in fact, the coupling extends over a larger range of R values and shows very strong angular dependence. The same occurs for the HF−He system (e.g., see Figure 2, middle panel), whereas the CO−He system shows a much weaker and short-ranged potential coupling, which also seems to be dependent very little on the orientational coordinate.

Such specific differences of the forces at play are seen, from the present calculation, to cause very direct differences in the corresponding behavior of the vibrational relaxation cross sections at collision energies down to $\sim 10^{-7}$ cm^{-1} (see Section IV). First of all, we find that, for all three cases, the Wigner's law regime is achieved over the range of considered energies, producing $\Delta\nu = 1$ relaxation cross-section limiting values for the LiH molecular partner, which are $\sim$2 or 3 orders of magnitude larger than those in the case of HF and 5 or 6 orders of magnitude larger than those for the CO molecule. Furthermore, the single quantum ($\Delta\nu = 1$) relaxation process from $\nu = 2$ that have also been analyzed in our calculations indicate again a very marked dominance of the efficiency shown by LiH (rates of $10^{-11}-10^{-12}$ cm^3·s^{-1}), with respect to those observed for HF (rates of $10^{-15}-10^{-16}$ cm^3·s^{-1}) and even more with respect to the very weakly coupled CO−He system (rates of $\sim 10^{-19}$ cm^3·s^{-1}). For a simple, semiclassical model of the vibrational relaxation process in which two distinct regimes (Bethe−Wigner at low collision energies and Landau−Teller at high collision energies) are distinguished and discussed, see the work of Dashevskaya et al.[40] However, note that, in that paper, the molecule is forced to remain in the $j = 0$ state. A more complex angular momentum arrangement in the outgoing waves might modify the picture in the intermediate energy range. Therefore, our own findings clearly suggest that the LiH molecule could indeed provide a much better candidate for its sympathetic cooling by collisions in a cold buffer gas of helium than could be achieved with either CO or HF. This is a piece of information that we expect should play a significant role in the planning of possible experiments.

Another interesting result from our present calculations is provided by the features of the scattering length (the real portion), as obtained from the limiting behavior of the computed

S-matrix elements. The CO−He and HF−He systems indicate negative values of the real portion of the scattering length for molecules initially in $\nu = 1$ and $\nu = 2$, whereas such negative values are absent in the case of the LiH−He system. As a consequence of this condition, the corresponding elastic cross sections in the former systems show a marked Ramsauer-type minimum at energies of $10^{-1}-10^{-2}$ cm^{-1}, whereas this minimum is absent in the case of LiH−He. This means that, around such energy values, the decrease in the cross-section size will consequently reduce the cooling efficiency of the collision processes for CO and HF; this reduction will not occur for LiH. This difference will therefore provide another advantage for the latter case, making it an even more attractive candidate for possible experimental studies.

In conclusion, we feel that our present study, although chiefly a computational study without, as yet, any experimental verification for its findings, provides however useful indications on the relative efficiency of collisional cooling rates of vibrationally excited molecules in ultracold gaseous mixtures where helium is employed as a buffer gas. Our calculations thus are determined to be capable of selecting one specific molecular candidate (i.e., the LiH molecule in its ground electronic state) as a possible choice for performing experimental verifications of its cooling efficiency.

Acknowledgment. This work is affectionately dedicated to Professor Donald H. Kouri, an outstanding scientist and a dear friend, on the occasion of his 60th birthday. We warmly wish him many more years of active and happy research endeavors. The financial support from the Italian Ministry for University and Research (MUIR), from the University of Rome "La Sapienza" Research Committee and from the INFM Computing Grant Committee is gratefully acknowledged. We are also grateful to Alex Dalgarno and N. Balakrishnan for several illuminating discussions on collisional cooling processes. Finally, we warmly thank Professor Ad Van der Avoird and Professor Brian Taylor for kindly sending us their computed potential energy surfaces for the HF−He and LiH−He systems, respectively.

Note Added after ASAP Posting. This article was published on the Web on 5/23/2003 with a minor error in the calculations; the author has since corrected the error in this version. The corrected data affected Table 1, Figures 3 and 7, and some text in Section IV, "Vibrational Relaxation Dynamics". The spelling of the name of Professor Ad Van der Avoird has also been corrected in the Acknowledgment. The corrected version was posted on 8/28/2003.

References and Notes

(1) Doyle, J. M.; Friedrich, B. *Nature* **1999**, *401*, 749.
(2) Wynar, R.; Freeland, R. S.; Han, D. J.; Ryu, C.; Heinzen, D. J. *Science* **2000**, *287*, 1016.
(3) Williams, C.; Julienne, P. *Science* **2000**, *287*, 986.
(4) Levi, B. G. *Phys. Today* **2000**, *53*, 46.
(5) Meijer, G. *ChemPhysChem* **2002**, *3*, 495.
(6) Arndt, M.; Nair, O.; Vos-Andreae, J.; Keller, C.; van der Zouw, G.; Zeilinger, A. *Nature* **1999**, *401*, 680.
(7) DeMille, D.; Bay, F.; Bickman, S.; Kawall, D.; Krause, D., Jr.; Maxwell, S. E.; Hunter, L. R. *Phys. Rev. A* **2000**, *61*, 052507.
(8) Gabbanini, C.; Fioretti, A.; Lucchesini, A.; Gozzini, S.; Mazzoni, M. *Phys. Rev. Lett.* **2000**, *84*, 2814.
(9) Nikolov, A. N.; Enscher, J. R.; Eyler, E. E.; Wang, H.; Stwalley, W. C.; Gould, P. L. *Phys. Rev. Lett.* **2000**, *84*, 246.
(10) Dion, C.; Drag, C.; Dulieu, O.; Tolra, B. L.; Masnou-Seeuws, F.; Pillet, P. *Phys. Rev. Lett.* **2001**, *86*, 2253.
(11) Tolra, B. L.; Drag, C.; Pillet, P. *Phys. Rev. A* **2001**, *64*, 61401R.
(12) Bethlem, L. H.; Berden, G.; Meijer, G. *Phys. Rev. Lett.* **1999**, *83* (8), 1558.
(13) Maddi, J. A.; Dinneen, T. P.; Gould, H. *Phys. Rev. A* **1999**, *60* (5), 3882.
(14) Bethlem, L. H.; Berden, G.; Crompvoets, F. M. H.; Jongma, R. T.; van Roij, A. J. A.; Meijer, G. *Nature* **2000**, *406*, 491.
(15) Doyle, J. M.; Friedrich, B.; Kim, J.; Patterson, D. *Phys. Rev. A* **1995**, *52* (4), 2515.
(16) Weinstein, J.; deCarvalho, R.; Guillet, T.; Friedrich, B.; Doyle, J. M. *Nature* **1998**, *395*, 148.
(17) Friedrich, B.; Weinstein, J. D.; deCarvalho, R.; Doyle, J. *J. Chem. Phys.* **1999**, *110*, 2376.
(18) Heijmen, T. G.; Moszynski, R.; Wormer, P.; van der Avoird, A. *J. Chem. Phys.* **1997**, *107*, 9921.
(19) Moszynski, R.; Wormer, P. E.; Jeziorski, B.; van der Avoird, A. *J. Chem. Phys.* **1994**, *101*, 2811.
(20) Taylor, B. K.; Hinde, R. J. *J. Chem. Phys.* **1999**, *111*, 973.
(21) Antonova, S.; Lin, A.; Tsakotellis, A. P.; McBane, G. C. *J. Chem. Phys.* **1999**, *110* (5), 2384.
(22) Bodo, E.; Gianturco, F. A.; Martinazzo, R.; Paesani, F.; Raimondi, M. *J. Chem. Phys.* **2000**, *113* (24), 11071.
(23) Krems, R. V. *J. Chem. Phys.* **2002**, *116*, 4517.
(24) Krems, R. V. *J. Chem. Phys.* **2002**, *116*, 4525.
(25) Martinazzo, R.; Bodo, E.; Gianturco, F. A. *Comput. Phys. Commun.* **2003**, *151*, 187.
(26) Calogero, F. *Variable Phase Approach to Potential Scattering*; Academic Press: New York, 1967.
(27) Pack, R. T. *J. Chem. Phys.* **1974**, *60* (2), 633.
(28) Abramowitz, M.; Stegun, I. A. *Handbook of Mathematical Functions*; Dover Publications, Inc.: New York, 1972.
(29) Taylor, J. R. *Scattering Theory: The Quantum Theory of Nonrelatistic Collisions*; Robert E. Krieger Publishing Company: Malabar, FL, 1969.
(30) Balakrishnan, N.; Kharchenko, V.; Forrey, R. C.; Dalgarno, A. *Chem. Phys. Lett.* **1997**, *280*, 5.
(31) Balakrishan, N.; Forrey, R.; Dalgarno, A. *Chem. Phys. Lett.* **1997**, *280*, 1.
(32) Manolopoulos, D. E. *J. Chem. Phys.* **1986**, *85* (11), 6425.
(33) Field, D.; Masden, L. B. *J. Chem. Phys.* **2003**, *118*, 1679.
(34) Zhu, C.; Balakrishnan, N.; Dalgarno, A. *J. Chem. Phys.* **2001**, *115* (3), 1335.
(35) Balakrishnan, N.; Dalgarno, A.; Forrey, R. C. *J. Chem. Phys.* **2000**, *113* (2), 621.
(36) We report here only the rotationally summed cross section, as obtained by $\sigma^q(\nu,j=0\rightarrow\nu') = \sum_{j'}\sigma(\nu,j=0\rightarrow\nu',j')$.
(37) Gianturco, F. A. *Collision Theory of Atoms and Molecules*; Plenum Publishing Company: New York, 1989.
(38) Bodo, E.; Gianturco, F. A.; Dalgarno, A. *Chem. Phys. Lett.* **2002**, *353*, 1.
(39) Cecchi-Pestellini, C.; Bodo, E.; Balakrishnan, N.; Dalgarno, A. *Astrophys. J.* **2002**, *571*, 1015.
(40) Dashevskaya, E. I.; Kunc, J. A.; Nikitin, E. E.; Oref, I. *J. Chem. Phys.* **2003**, *118*, 3141.